2014 IEEE International Conference on Robotics & Automation (ICRA)
Hong Kong Convention and Exhibition Center
May 31 - June 7, 2014. Hong Kong, China

Adaptive Synergy Control of a Dexterous Artificial Hand to Rotate Objects in Multiple Orientations Via EMG Facial Recognition

Benjamin A. Kent, Zahi M. Kakish, Nareen Karnati, and Erik D. Engeberg

***Abstract*—An adaptive synergy controller is presented which allows a dexterous artificial hand to unscrew and screw an object using facial expressions derived from electromyogram (EMG) signals. In preliminary experiments, the finger joint motions of nine human test subjects were recorded as they unscrewed a bottle cap in multiple orientations of their hands with respect to the object. These data were used to develop a set of adaptive sinusoidal joint synergies to approximate the orientation-dependent human motions, which were then implemented on a dexterous robotic manipulator via the proposed adaptive synergy controller. The controller is driven through a noninvasive interface which allows a single input to drive the bioinspired human motions using facial expressions. The adaptive synergy controller was evaluated by four able-bodied subjects who were able to unscrew and screw an instrumented object using the artificial hand in two orientations with a 100% success rate.**

***Index Terms*— Dexterous Hand, Electromyogram (EMG), and Grasp Synergy**

I. Introduction

Despite the advances in the mechanical dexterity [1, 2] and sensory feedback [3, 4] of robotic hands, disabled people often cannot fully make use of the increased functionality of these manipulators. This is usually due to the lack of an intuitive and robust interface between the human and the artificial hand. Recently, the use of noninvasive brain-machine interfaces (BMIs) using electroencephalogram (EEG) signals have been investigated as a method of control for robotic systems [5]. One current problem with BMIs is that the number of independent inputs that can be extracted to control an artificial hand is limited. To help simplify the problem, the concept of grasp synergies has been explored, where a limited number of control inputs are used to specify the action of a larger number of joints [6, 7]. Therefore, grasp synergies are an important consideration to reduce the cognitive burden of disabled people to control a dexterous artificial hand. Proper use of grasp synergies can enable people to control very dexterous motions of artificial hands with a single input.

Synergistic control strategies exist in various forms, i.e. postural [8], force [9], and temporal [10]. The latter of these three types, temporal, is particularly relevant to the current work. Underlying this approach is the idea that the CNS utilizes temporal coordination between muscle groups to achieve a given task [11]. This idea enables a viable solution to a serious problem for quadriplegic victims, which is that the information throughput to the artificial hand from the operator is quite small regardless of the control interface that is used.

Often, BMIs for disabled people make use of the fact that the power in different frequency bands of EEG can increase or decrease before, during and after real and imagined hand movements; these are called event related synchronization (ERS) and event related desynchronization (ERD) [12, 13].

There are a number of problems associated with BMIs that use ERD and ERS to assess the intent of the operator. For example, they are susceptible to external visual stimuli, motion artifacts, and blinking, requiring advanced signal processing techniques to function [14]. The successful signal classification rates are often in the 70%-90% range and there is a great deal of inter-subject variability; some users cannot generate the necessary ERD and ERS signals to control BMIs [15]. The training time to become a proficient operator can also be substantial and the time delays in the BMIs required to adequately filter the low amplitude EEG signals can be lengthy.

In the present work, an adaptive synergy controller is proposed and applied to a dexterous robotic hand to unscrew and screw objects in multiple orientations. The synergy controller is designed to require only a single input from the operator, which is obtained from EMG signals corresponding to the facial expressions of the subjects. This enables a high successful classification rate from the subjects and a very short training time required to learn to unscrew and screw objects with an artificial hand in different orientations. Thus, the prime application for this technique would be to assist quadriplegic victims in their daily tasks of life. The use of EMG also provides a robust and speedy classification system, which is a problem with BMIs that rely on EEG [15].

To develop this synergy controller, the hand motions of nine human test subjects were recorded while unscrewing a bottle cap in multiple orientations during preliminary experiments. These motions were used to derive variable-amplitude sinusoidal joint synergies to approximate the human motions depending upon the orientation between the hand and object (Fig. 1(a)) (Section III) [1]. From these, the proposed

Manuscript received September 15, 2013. This research supported in part by the National Science Foundation award #1317952.

B. A. Kent is currently pursuing his PhD at University of Akron, Akron, OH 44325 USA (phone: 330-998-4122; e-mail: bak17@ zips.uakron.edu).

Z. M. Kakish is currently a Master of Science student with the Mechanical Engineering Department at the University of Akron, Akron, OH 44325 USA (e-mail: zmk5@zips.uakron.edu)

N. Karnati, has recently completed the Master of Science degree from Mechanical Department at the University of Akron, Akron, OH 44325 USA (e-mail: nk29@zips.uakron.edu).

E. D. Engeberg has joint appointments with the Mechanical and Biomedical Engineering Departments at the University of Akron, Akron, OH 44325 USA, (e-mail: engeberg@uakron.edu).

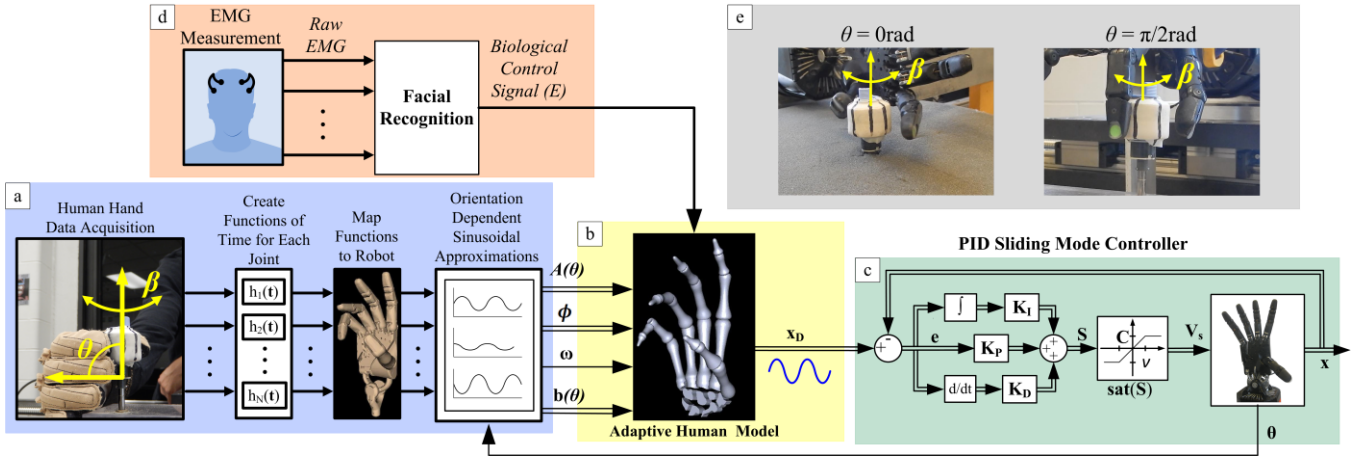

Fig. 1. Top level block diagram of the Adaptive Synergy Controller. (a) In preliminary work, a set of orientation-dependent sinusoidal joint approximations were developed from observed human tendencies (b) The Adaptive Human Model controller utilizes the previously derived synergies and biological control signal *E* to determine the vector of desired sinusoidal joint angles ($\boldsymbol{x_D}$) for the Shadow Hand. (c) The human adaptive synergies were implemented on the C6M Dexterous Shadow Hand via a PID sliding mode controller. (d) A headset is used to create a biological control signal used to drive the screwing and unscrewing synergies based on the facial expressions of test subjects. (e) The proposed controller was evaluated by four able-bodied subjects who used the Shadow Hand to screw and unscrew an instrumented object in multiple orientations.

Adaptive Synergy Controller was developed (Fig. 1(b)) and then implemented on the C6M Dexterous Shadow Hand (Section IV) via a robustly stable PID sliding mode controller (Fig. 1(c)). Operation of the Adaptive Synergy Controller is achieved via a non-invasive facial expression classifier using EMG signals measured bilaterally from the scalp (Fig. 1(d)). The current study expands upon previous work [1] by considering multiple orientations, and in addition investigates two separate methods of facial expression signal processing within the proposed adaptive control framework. Sections V and VI describe the experimental methods and results, as the timed task was repeated with the Shadow Hand using the adaptive synergy controller to unscrew and screw an instrumented object in multiple orientations (Fig. 1(e)).

II. Equipment

A. CyberGlove II

The CyberGlove II (CyberGlove Systems, Inc.) records joint angle data of the human hand in real time. While the glove itself contains 22 sensors, only those associated with the first finger and thumb are used in the current work. The first finger of the CyberGlove contains four sensors, two of which record joint angle data for distal interphalangeal (DIP) and proximal interphalangeal (PIP) joints (FJ1a and FJ1b). The remaining two measure the extension/flexion (FJ2) and abduction/adduction (FJ3) of the metacarpophalangeal (MCP) joint. For the thumb, TJ1 and TJ2 measure the flexion/extension of the DIP and MCP, respectively. Sensors TJ3 and TJ4 of the CyberGlove respectively record the abduction and circumduction angles of the carpometacarpal (CMC) joint of the thumb (Fig. 2(a)). This joint convention was chosen to correlate with the kinematic model of the C6M Dexterous Shadow Hand (Fig. 2(b)).

B. The C6M Dexterous Shadow Hand

The C6M is a dexterous underactuated tendon-driven anthropomorphic robotic hand with 24 joints and 20 DOFs. However, in this paper only eight joints are used from the first finger and thumb (Fig. 2(b)). A system model for the Shadow Hand can be obtained through a summation of torques:

$$\boldsymbol{I\ddot{x} + B\dot{x} + Kx + D = \tau}. \quad (1)$$

The effective inertia ($\boldsymbol{I} \in \mathbb{R}^{nxn}$), stiffness ($\boldsymbol{K} \in \mathbb{R}^{nxn}$) and damping ($\boldsymbol{B} \in \mathbb{R}^{nxn}$) are subject to change as the system establishes and loses contact with the environment. The angular position, velocity, and acceleration are $\boldsymbol{x}$, $\boldsymbol{\dot{x}}$, and $\boldsymbol{\ddot{x}}$. $\boldsymbol{\tau} \in \mathbb{R}^n$ are the torques supplied by the motors and $\boldsymbol{D} \in \mathbb{R}^n$ are the unknown disturbance torques.The orientation of the Shadow Hand (θ) was ascertained from a three axis accelerometer mounted on the back of the palm.

III. Human Finger Joint Synergies

A. Experimental Methods: Human Experiments

In preliminary experiments, nine human test subjects were asked to unscrew a bottle cap with their thumb and first finger while wearing the CyberGlove II to record the motions (Fig.

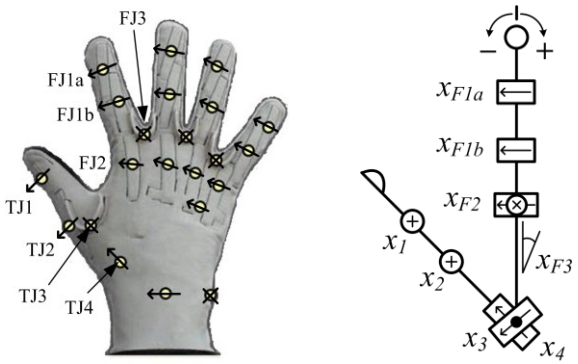

(a) (b)

Fig. 2. (a) The CyberGlove II has 22 sensors to measure the motions of human hands. Axes of rotation are visualized as black arrows. Axes of rotation perpendicular to the page are designated by an (**X**). (b) The kinematic diagram of the thumb and first finger of the Shadow Hand.

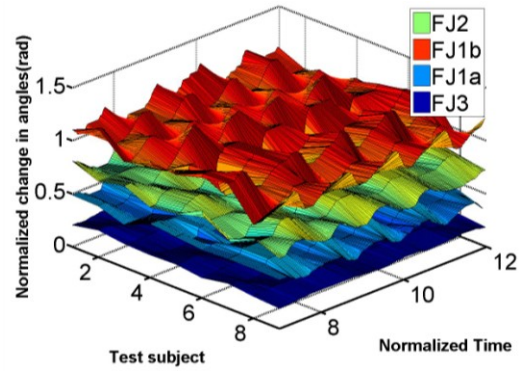

(a)

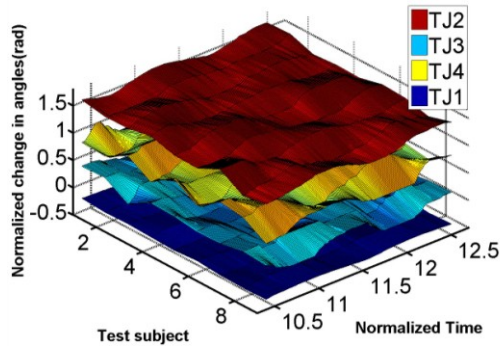

(b)

Fig. 3. (a) Recorded first finger joint angle data when the orientation angle θ = 0rad. Presented data represents all nine test subjects. (b) Recorded thumb joint angle data in the θ = π/2rad orientation.

1(a)). All subjects participated with informed consent in accordance with IRB protocol. Each test subject was first fitted with a brace to immobilize the wrist during testing. Prior to data acquisition, the forearm of each subject was secured in place and a bottle was placed at a measured orientation angle (θ) relative to the wrist. Here, the orientation angle is defined as the angle between the axis of rotation of the bottle cap and the longitudinal axis of the forearm that runs from the elbow to the hand (Fig. 1(a)). Each subject was then asked to unscrew the bottle cap with their first finger and thumb while finger joint angle data were recorded. This procedure was performed five times by each participant as the orientation angle (θ) between the bottle and the wrist was varied from 0 to π/2rad. Experimental data were recorded at orientation angles of 0, π/8, π/4, 3π/8, and π/2rad for each test subject.

B. Results: Joint Space Analysis

All joint angle data were first filtered and normalized with respect to time. Contour plots from a single trial for each subject were constructed for each joint while in the θ = 0rad (Fig. 3(a)) and θ = π/2rad (Fig. 3(b)) orientations. These plots show all joint angles for each test subject with respect to normalized time as the unscrewing task was performed. As observed for each trial, the relative amplitude of motion is comparable between subjects, and the frequency of motion for each joint remains largely constant for each trial. As with prior experiments, the joint angle motions of the test subjects strongly resemble sinusoids (Fig. 3) [16]. This sinusoidal trend was consistent with all the data for all values of θ.

Next, a principal component analysis (PCA) was performed to determine the impact of each joint on the unscrewing motion with respect to the orientation angle, θ. A PCA on the thumb and first finger joints shows a very similar approach taken by each test subject, as in [16]. However, as the orientation of the bottle varied from 0 to π/2rad, the amount of contribution that each joint had upon the overall motion of the synergy varied substantially. The contribution of each joint (i.e. the percentage of variance in the data attributed to that joint in each trial) obtained by the PCA was averaged across all subjects at five different values of θ while using the thumb and first finger to unscrew the bottle cap (Fig. 4). Joints FJ1b, FJ2, and TJ1 contribute strongly to the motion, while the influence of joint TJ2 was less significant. Joint TJ3 (the abduction joint) of the thumb had a stronger impact upon the motion with large values of θ while FJ2, and FJ1b (the extension joints) were more influential with small values of θ.

From Fig. 4, it can be seen that the percentage contribution of some joints exhibit a nearly linear relationship with varying values of θ. A best fit line was determined for the percentage contribution of each joint at each recorded orientation angle resulting in five data points per set, and the r-squared values were calculated (Fig. 4). A strong correlation is seen for joints FJ1b, TJ3, and TJ4. Lower r-squared values were obtained for joints TJ2 and FJ3, however these remain relatively constant for all θ values and do not contribute strongly to the variance in the motion. These results indicate that the test subjects used different motor control strategies to unscrew the object in different orientations (θ) of the hand with respect to the bottle.

From the PCA data, a set of sinusoidal trajectories were developed to approximate the recorded human motions. This was accomplished by approximating the motion of each joint as a single sine wave with an orientation-dependent amplitude:

$$x_{D_k} = A_k(\theta)sin(\omega t + \phi_k) + b_k(\theta). \qquad (2)$$

In (2), the desired sinusoidal approximation of joint k (x_{D_k}) is determined by appropriate choice of the amplitude ($A_k(\theta)$), phase offset (ϕ_k) and position offset ($b_k(\theta)$). The relative speed of each approximation is determined by the frequency (ω). For more information on this process, see [1]. To

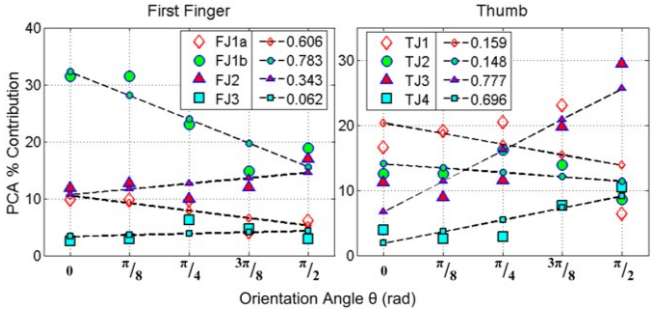

Fig. 4. The PCA data from each test subject averaged together at five different values of θ shows that the orientation angle, θ, significantly affects the motor control strategy of the test subjects. Larger markers indicate the average percent contribution to the motion at each θ value, while the smaller markers with dashed lines denote the best-fit line approximation for the respective joint. The r-squared value for each linear approximation is given in the legend.

facilitate the versatile application of this adaptive human grasp strategy with a dexterous robotic hand, a set of linear equations were developed to scale the amplitudes of the sinusoids (A_k) and offsets (b_k) as a function of the orientation angle θ (TABLE I), described further in Section IV. The sinusoidal approximations produce fingertip trajectories in the Cartesian space that are periodic on 2π.

Previous work has shown that the same set of sinusoidal trajectories can be used to produce both unscrewing and screwing motions at the fingertips [1]. This is achieved by reversing the direction of the time vector t in (2) used to drive the sinusoids. This produces the same Cartesian trajectories of the fingertips, but mirrored in time. An increasing time vector produces unscrewing motions, while a decreasing time vector produces screwing motions. This feature is used in the current work to impart both directions of motion to an object in multiple orientations.

A joint space error analysis was performed to determine how well the approximated sinusoids represented the actual recorded human joint motions for the first finger. Two cycles of each trial, normalized with respect to time, were extracted from each trial for comparison with the sinusoidal approximations, and the absolute relative error was calculated (Fig. 5). Across all orientations for all joints, the average error in joint space remains less than 0.1rad. This suggests that the derived sinusoidal approximations (TABLE I) accurately reflect the differing manipulation strategies adopted by the human test subjects as the orientation angle θ varied. This adaptive sinusoidal synergy approximation was next applied to the Shadow Hand (see [1] for more details on this process).

IV. Shadow Hand Adaptive Synergy Controller

A. Adaptive Synergy Controller

The desired position ($\boldsymbol{x_D}$) for the adaptive synergy controller is of the form

$$\boldsymbol{x_D} = \boldsymbol{A}(\theta)\boldsymbol{u} + \boldsymbol{b}(\theta) \tag{3}$$

where $\boldsymbol{A}(\theta) \in \mathbb{R}^{nxn}$ is an adaptive diagonal matrix

$$\boldsymbol{A}(\theta) = \begin{bmatrix} A_1(\theta) & \cdots & 0 \\ \vdots & \ddots & \vdots \\ 0 & \cdots & A_n(\theta) \end{bmatrix}, \tag{4}$$

and $\boldsymbol{u} \in \mathbb{R}^n$ is a vector of sinusoids:

$$\boldsymbol{u} = [\sin(\omega E + \phi_1) \cdots \sin(\omega E + \phi_n)]^T. \tag{5}$$

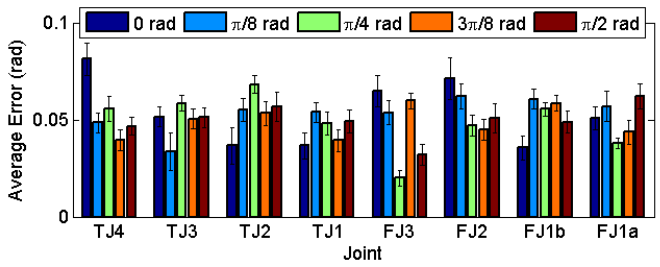

Fig. 5. Joint Space Error Analysis between CyberGlove data and desired sinusoidal approximations (2) for the first finger and thumb.

TABLE I: SINE WAVE SCALING PARAMETERS (RAD)

Joint	Phase Offset φ_k	Position Offset $b_k(\theta)$	Amplitude $A_k(\theta)$
x_{F1}	0.800	0.795	0.520 – 0.07θ
x_{F2}	0.000	0.370	0.405 – 0.16θ
x_{F3}	1.571	0.000	0.000 - 0.20θ
x_1	0.305	0.390	0.200 - 0.15θ
x_2	0.000	0.140	0.250 – 0.05θ
x_3	1.070	0.698+0.111θ	0.050 + 0.20θ
x_4	-0.000	0.349+0.055θ	0.000

E is a scalar input based on measured EMG signals used to drive the adaptive synergy controller, and is explained in further detail subsequently. ω is an arbitrary scalar value used to scale the frequency of the sinusoidal joint motions relative to the input, E. $\boldsymbol{b} \in \mathbb{R}^n$ is a vector of joint angle offsets:

$$\boldsymbol{b}(\theta) = [b_1(\theta) \cdots b_n(\theta)]^T. \tag{6}$$

The phase shift, ϕ_k, and joint angle offset, $b_k(\theta)$, for any joint k, are determined from the observations of the human data and are included in TABLE I. The controller for the Shadow Hand can be visualized as in Fig. 1. The input to the adaptive synergy controller, E in (5), can be thought of as a "time" vector which temporally synchronizes the cyclic motions of the joints which are periodic on 2π.

B. PID Sliding Mode Controller

To facilitate sliding mode control, an error state vector is defined as $\boldsymbol{e} = \boldsymbol{x_D} - \boldsymbol{x}$. The PID sliding mode control law for the Shadow Hand is written as

$$\boldsymbol{V_s} = -\boldsymbol{C}sat(\boldsymbol{K_I}\int \boldsymbol{e}dt + \boldsymbol{K_P}\boldsymbol{e} + \boldsymbol{K_D}\dot{\boldsymbol{e}}), \tag{7}$$

where $\boldsymbol{V_S} \in \mathbb{R}^{nxn}$ is the voltage input vector to the motors (Fig. 1). $\boldsymbol{C} \in \mathbb{R}^{nxn}$ is a diagonal matrix that is chosen as an upper bound estimate on the motor voltages required to overcome the torques applied to the joints of the Shadow Hand that are involved in the synergies. $\boldsymbol{K_I} \in \mathbb{R}^{nxn}$, $\boldsymbol{K_P} \in \mathbb{R}^{nxn}$, and $\boldsymbol{K_D} \in \mathbb{R}^{nxn}$ are the diagonal integral, proportional and derivative gain matrices, respectively. The ***sat*** function partially linearizes the control law to alleviate the chattering phenomenon that is common with mechanical systems that use a fully nonlinear control law associated with the signum function [17].

V. Methods: Shadow Hand

A. Biological Signal Measurement

EMG signals were recorded using the Emotiv Systems, Inc. (San Fransisco, USA) EPOC wireless headset. The EPOC headset contains 16 sensors for measuring EMG and EEG signals and has a 128Hz sampling frequency. The locations of the sensors correspond to the 10-20 system [14]. Using the EPOC headset, two separate methods of control with the recorded EMG signals were developed for use with the proposed Adaptive Synergy Controller. Both methods utilize the Emotiv EPOC software development kit (SDK), which recognizes different facial expressions using EMG signals.

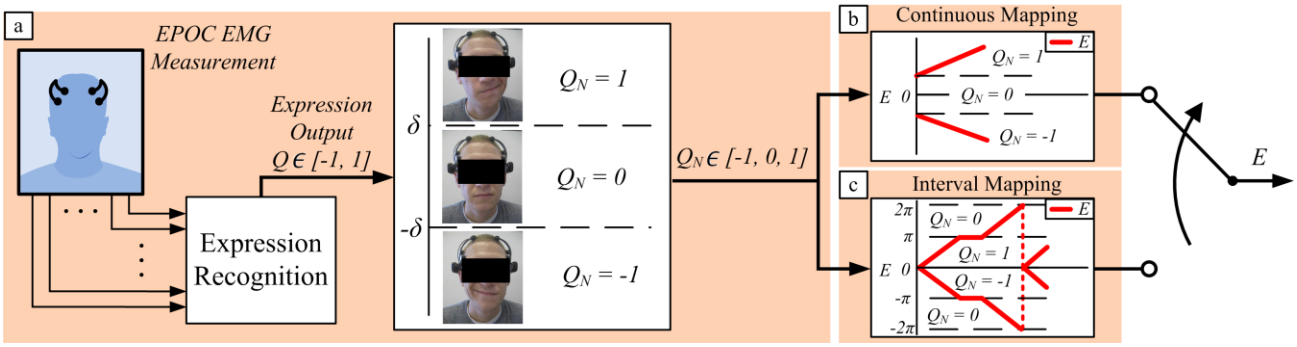

Fig. 6. (a) The EPOC system converts registered facial expressions into a continuous, normalized output signal (Q) relative to the intensity of the expression. A threshold classifier is implemented on the output signal Q to convert to the signal to a tertiary on-off-on signal (Q_N). This promotes smoother operation of the Adaptive Synergy Controller. The resulting signal Q_N is then used to drive the two separate mapping methods (b) The Continuous mapping continuously increments or decrements the value of the input E (5) while Q_N is nonzero. (c) The Interval mapping requires intermittent expression and relaxation of the face to properly execute the desired motions. This method provides more direct control but requires more cognitive effort to operate effectively.

The EPOC software outputs a normalized signal proportional to the intensity of each registered facial expression.

To implement the proposed controller on the Shadow Hand, a LabVIEW VI was developed allowing the users' facial expressions to read by the EPOC SDK as a means of control. For bilateral expressions, the sign of the output is determined by which side of the face it is recognized on (i.e., a left smirk produces a negative signal, while a right smirk produces a positive signal). This property allows the creation of a proportional bipolar signal, Q (Fig. 6(a)), which was used to drive the Shadow Hand. This bipolar signal was passed through a threshold classifier to convert the proportional signal to a three state on-off-on output ($Q_N \in [-1,0,1]$). The resulting signal was then used as the input to two separate mapping methods (Fig. 6(b,c)), which impart different types of control. In the current work, smiling is utilized in a bilateral manner to drive the Adaptive Synergy Controller. A smirk on the right side of the face produces unscrewing, while a smirk on the left side of the face produces screwing motions.

B. Method One – Continuous Mapping

The first mapping method considered herein is termed Continuous mapping. In this approach, the input E functions as a monotonically increasing or decreasing vector used to drive the sinusoidal joint approximations (3), (5). E is initialized to zero when the controller is started. While Q_N remains zero, the 'time' vector E remains at its previous value. When an expression is recognized (Q_N = -1, 1), the input E is incremented or decremented according to the sign of the expression output Q_N (Fig. 6(b)). This technique is presented in the form of pseudocode in Fig. 7(a). The Continuous mapping method requires little cognitive effort to properly operate, but requires a constant input signal to produce rotation of the object.

C. Method Two – Interval Mapping

The second mapping method builds upon the first method. In this approach, the control input E is defined piecewise linearly in halves. For both screwing and unscrewing motions, the first half of the synergy ($E = 0 \rightarrow \pm\pi$) is executed when the appropriate facial expression is recognized (Q_N = -1, 1). The second half of the synergy ($E = \pm\pi \rightarrow \pm 2\pi$) is then performed autonomously once the expression is released and the face returns to neutral (Fig. 6(c)). Upon completion of the second half of the synergy, the control input E is reset to zero via a modulo operation. This relationship is described mathematically by the pseudocode representation in Fig. 7(b). The result of this mapping is that the operator rhythmically generates and releases the appropriate facial expression to produce the desired rotational motion of the object. This technique requires more cognitive effort from the operator, but does not require constant expression of the face to produce rotation. This offers more direct control to the operator and possibly reduces the effect of fatigue relative to the first method, which requires a sustained expression to operate.

D. Experimental Methods – Human Evaluation

Both mapping methods were evaluated by four able-bodied test subjects, who participated with informed consent in accordance with IRB protocol. Each participant underwent two separate testing sessions. Each participant was fitted with the EPOC headset, and the threshold values (δ, Fig. 6) were tuned for each user. After calibration, the subjects underwent a five minute training period to familiarize themselves with the

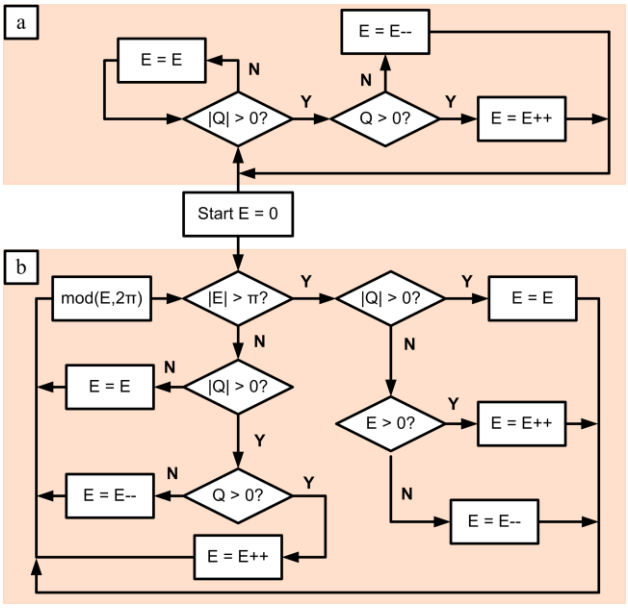

Fig. 7. (a) Pseudocode representation of the Continuous mapping method, which requires a sustained expression to produce rotational motion of an object. (b) Pseudocode representation of the Interval mapping method. The control logic considers the synergy in two halves, requiring a cyclic expression and release to drive the controller.

system. During the first testing session, the Shadow Hand was mounted in the θ = 0rad orientation (Orientation 1) (Fig. 1(e)), with a potentiometer mounted to a cylinder to measure the angular position (β) of rotation. Each participant underwent five trials with each mapping method, resulting in 10 trials per subject per session. Each trial consisted of screwing and unscrewing the potentiometer across its range of motion (~1.5πrad). During the second session, the Shadow Hand was mounted in the θ = π/2rad orientation (Orientation 2) and the above process was repeated (Fig. 1(e)).

After data acquisition, the time to complete the individual screwing and unscrewing motions were tabulated for each trial. The average completion time data for each subject were evaluated using a two factor ANOVA test for the screwing and unscrewing motions separately. The ANOVA test evaluated the influence of orientation (factor A) and mapping method (factor B) in the performance of the controller.

VI. Results: Shadow Hand

An individual trial from the Continuous and Interval mapping methods in varying orientations are presented in Figs. 8 and 9, respectively. As can be seen in Fig. 8, a sustained expression increments or decrements the input E, producing rotation of the potentiometer. In contrast, the Interval mapping method (Fig. 9) requires intermittent expression and relaxation to execute a full cycle of the sinusoids. The orientation-dependent nature of the task is also apparent via comparison of the recorded joint angles in the bottom graph of each figure. While in Orientation 1, rotation of the object is performed primarily by the flexion/extension joints, with finger abduction (x_{F3}) playing a minor role (Fig. 8, bottom). This is reversed in Orientation 2, where finger abduction is required to produce rotational motion and the flexion/extension joints play a lesser role in the task (Fig. 9, bottom). An extracted photo sequence of the Shadow Hand performing the task in each orientation is presented in Fig. 10.

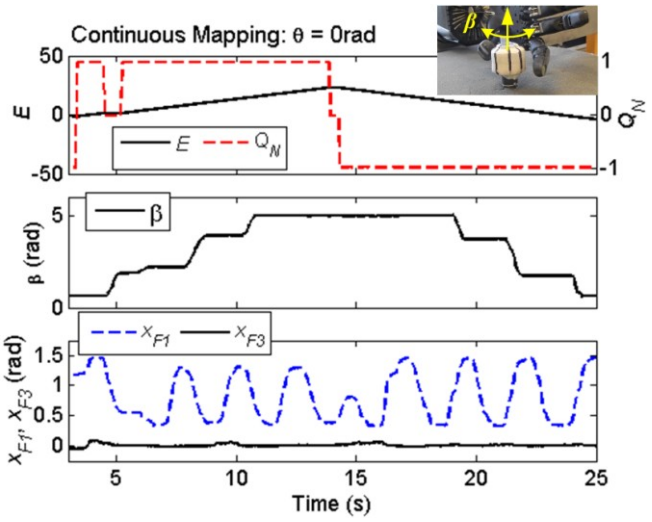

Fig. 8. Example trial of the Shadow Hand under the Continuous mapping while in Orientation 1. A sustained expression increments or decrements the 'time' vector E according the sign of the expression output Q_N. In this orientation, abduction/adduction of the first finger (x_{F3}) is not required to produce rotational motion. The flexion/extension joints of the finger (x_{F1}, x_{F2}) play a larger role in this orientation and are responsible for screwing and unscrewing the potentiometer.

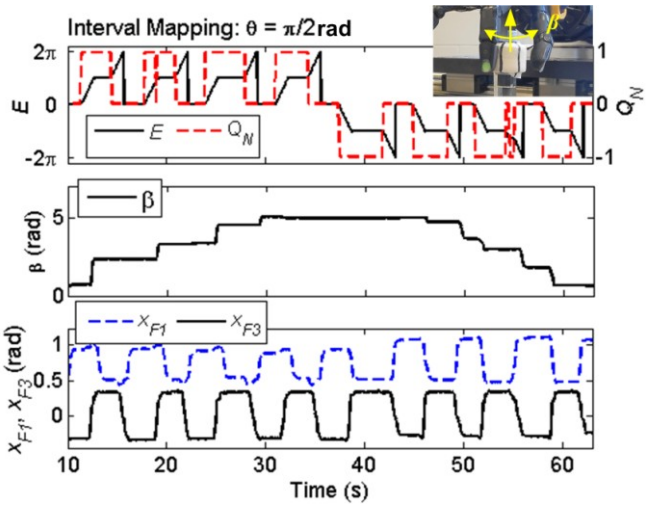

Fig. 9. Example trial of the Shadow Hand under the Interval mapping while in Orientation 2. Under this mapping scheme, the operator is required to intermittently express and relax the face to produce rotational motion of the object. Unlike Orientation 1, abduction/adduction of the first finger (x_{F3}) is required to produce rotational motion of the potentiometer, while the flexion/extension joints (x_{F1}, x_{F2}) play a diminished role in the task.

The completion time results of the Adaptive Synergy Controller evaluation are presented in Fig. 11. Results show that the Continuous mapping produced faster completion times for both orientations and motions (screwing, unscrewing). On average, the participants completed the tasks (both screwing and unscrewing) in 10.28s and 9.72s under the Continuous mapping method while in Orientation 1 and 2, respectively. Completion rates for the Interval mapping were slower, with mean times of 28.47s and 20.04s in Orientations 1 and 2, respectively (Fig. 11). The test subjects were able to complete all trials successfully.

The results of the performed ANOVA analyses are presented in Table II. The Continuous mapping was statistically faster than the Interval mapping method for both the unscrewing and screwing motions, indicating that the mapping method (factor B) proved a significant factor in completion time for both motions ($p_B < 0.001$). For the screwing motion, the orientation (factor A) was a significant factor in the performance of the controller, while the opposite was true for the unscrewing motion (Table II). This discrepancy may be caused by the compliance of the manipulator as the fingertip comes into contact with the surface of the potentiometer. In Orientation 1, the unscrewing and screwing motions require 'pulling' and 'pushing' motions during contact, respectively. This is not the case in Orientation 2, where the nature of the contact is similar between motions (contact is first established via finger flexion, followed by rotation of the object via ab/adduction of the finger) (Fig. 10).

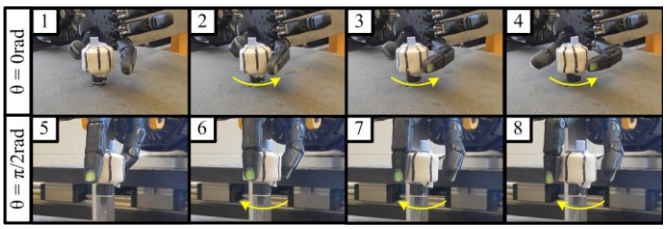

Fig. 10. Extracted photo sequence of the Shadow Hand testing while in Orientation 1 (top) and Orientation 2 (bottom).

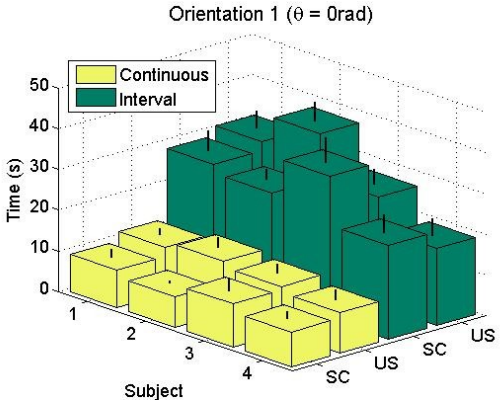

(a)

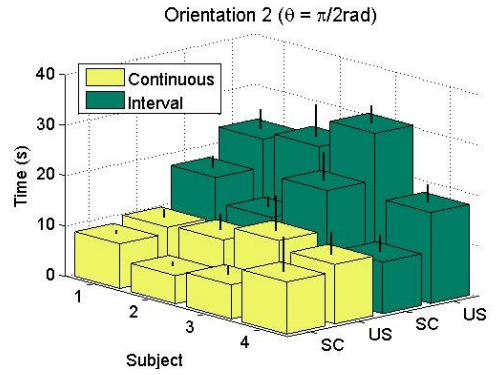

(b)

Fig. 11. Average completion times and standard deviations per subject with each mapping method (Continuous, Interval) for the screwing (SC) and unscrewing (US) motions. (a) In Orientation 1 (θ = 0rad) and (b) Orientation 2 (θ = π/2rad). The Continuous mapping method produced faster times in general, but all trials were successfully completed.

This is further supported by the significant interaction factor between orientation and mapping ($p_{A/B}$ = 0.0103) in the screwing task, while the interaction factor did not prove significant for the unscrewing task ($p_{A/B}$ = 0.4023) (TABLE II).

VII. CONCLUSION

An adaptive synergy controller was presented which uses EMG signals from facial expressions to unscrew and screw an object in multiple orientations with a dexterous robotic hand. Two separate facial expression mapping methods were considered, with the Continuous mapping producing statistically faster completion times. This bioinspired control architecture can also be adapted for use with other temporal synergies to generate other complex motions or complete additional tasks via a single input. Such an approach can be realized via other forms of parametric approximations of finger joint motions that are coordinated via a shared time vector [18]. This level of model-based adaptive control is very important to restore lost functionality due to the difficulty in obtaining many independent control channels from paralyzed individuals. As demonstrated in this paper, a single input can be used to perform a task in multiple orientations by using an adaptive synergy controller. EMG-based facial recognition was used as the input to this adaptive controller because it enabled all test subjects to complete each task 100% of time. This approach is more robust to motion artifacts such as blinking and requires less advanced processing techniques for reliable operation than EEG-based BMIs; however eventual fatigue of the facial muscles is a possible drawback. Future work involves development of a higher level controller, integrating other temporal synergies within a finite state machine-like architecture to enable the user to select between multiple tasks or functions to be performed.

TABLE II: ANOVA ANALYSIS - P VALUES

Motion	Factor		
	A	***B***	***A/B***
Screwing	0.0034	< 0.0001	0.0103
Unscrewing	0.4074	< 0.0001	0.4023

REFERENCES

[1] N. Karnati, B. A. Kent, and E. D. Engeberg, "Bioinspired sinusoidal finger joint synergies for a dexterous robotic hand to screw and unscrew objects with different diameters," *IEEE/ASME Trans Mechatron,* vol. 18, pp. 612-623, 2013.

[2] A. Deshpande, Z. Xu, M. Weghe, B. Brown, J. Ko, L. Chang, D. Wilkinson, S. Bidic, and Y. Matsuoka, "Mechanisms of the anatomically correct testbed hand," *IEEE/ASME Trans Mechatron,* vol. 18, pp. 238-250, 2011.

[3] J. Fishel and G. Loeb, "Bayesian exploration for intelligent identification of textures," *Frontiers in Neurorobotics,* vol. 6, pp. 1-20, 2012.

[4] K. Horch, S. Meek, T. Taylor, and D. Hutchinson, "Object discrimination with an artificial hand using electrical stimulation of peripheral tactile and proprioceptive pathways with intrafascicular electrodes," *IEEE Trans Neural Sys and Rehab Eng,* vol. 19, pp. 483-489, 2011.

[5] A. Ferreira, W. Celeste, F. Cheein, T. Bastos-Filho, M. Filho, and R. Carelli, "Human-machine interfaces based on emg and eeg applied to robotic systems," *J NeuroEng and Rehab,* vol. 5, pp. 1-15, 2008.

[6] R. Vinjamuri, M. Sun, C. Chang, H. Lee, R. Sclabassi, and Z. Mao, "Dimensionality reduction in control and coordination of the human hand," *IEEE Trans Biomed Eng,* vol. 57, pp. 284-295, 2010.

[7] J. Shim, M. Latash, and V. Zatsiorsky, "Prehension synergies: Trial-to-trial variability and hierarchical organization of stable performance," *Exp Brain Res,* vol. 152, pp. 173-184, 2003.

[8] M. Ciocarlie and P. Allen, "Hand posture subspaces for dexterous robotic grasping," *Int J Robotics Res,* vol. 28, pp. 851-867, 2009.

[9] M. Santello and J. Soechting, "Force synergies for multifingered grasping," *Exp Brain Res,* vol. 133, pp. 457-467, 2000.

[10] R. Vinjamuri, S. Mingui, C. Cheng-Chun, L. Heung-No, R. J. Sclabassi, and M. Zhi-Hong, "Temporal postural synergies of the hand in rapid grasping tasks," *IEEE Trans Info Tech in Biomedicine,* vol. 14, pp. 986-994, 2010.

[11] A. d'Avella, P. Saltiel, and E. Bizzi, "Combinations of muscle synergies in the construction of a natural motor behavior," *Nature Neuroscience,* vol. 6, pp. 300-308, 2003.

[12] R. Salmelin and R. Hari, "Spatiotemporal characteristics of sensorimotor neuromagnetic rhythms related to thumb movement," *Neuroscience,* vol. 60, pp. 537-550, 1994.

[13] G. Pfurtscheller and C. Neuper, "Event-related synchronization of mu rhythm in the eeg over the cortical hand area in man," *Neuroscience Letters,* vol. 174, pp. 93-96, 1994.

[14] S. Sanei and J. Chambers, *Eeg signal processing*. West Sussex, England: Wiley, 2007.

[15] L. Bi, X. Fan, and Y. Liu, "Eeg-based brain-controlled mobile robots: A survey," *IEEE Trans Human-Machine Sys,* vol. 43, pp. 161-176, 2013.

[16] N. Karnati, B. Kent, and E. Engeberg, "Backdrivable periodic finger joint synergies: Human observations applied to a dexterous robotic hand," in *IEEE Int Conf Robotics and Biomimetics*, Phuket Island, Thailand, 2011.

[17] E. D. Engeberg, "A physiological basis for control of a prosthetic hand," *Biomed Sig Proc and Control,* vol. 8, pp. 6-15, 2013.

[18] B. A. Kent, J. Lavery, and E. D. Engeberg, "Anthropomorphic control of a dexterous artificial hand via task dependent temporally synchronized synergies," *J Bionic Eng,* 2014, to be published.